Check for updates

High Power Laser Science and Engineering, (2026), Vol. 14, e67, 9 pages.
doi:10.1017/hpl.2026.10165

HIGH POWER LASER SCIENCE AND ENGINEERING

RESEARCH ARTICLE

High-power high-efficiency room-temperature terahertz sources in lithium niobate crystals

Xieqiu Yu[1,†], Deyin Kong[1,2,3,†], Jiahua Cai[1], Jianghao Li[1,2], Aojie Xu[1], Deepak Suthar[1], Tong Chen[1], Baolong Zhang[4,5], and Xiaojun Wu[1,2,3]

[1]*Hangzhou International Innovation Institute, Beihang University, Hangzhou, China*

[2]*School of Electronic and Information Engineering, Beihang University, Beijing, China*

[3]*Zhangjiang Laboratory, Shanghai, China*

[4]*Division of Physics and Applied Physics, School of Physical and Mathematical Sciences, Nanyang Technological University, Singapore, Singapore*

[5]*Centre for Disruptive Photonic Technologies, The Photonics Institute, Nanyang Technological University, Singapore, Singapore*

(Received 18 January 2026 UTC; revised 30 March 2026 UTC; accepted 26 May 2026 UTC)

Abstract

High-power terahertz (THz) pulses are important for material analysis and ultrafast spectroscopy, but existing sources barely achieve high field strength and average power simultaneously. Tilted-pulse-front pumping (TPFP) improves THz conversion efficiency, but its optimal configuration is highly dependent on pump parameters. Focusing on high single-pulse energy (millijoule level) and a short pulse duration (226 fs), this study systematically evaluates two TPFP configurations: the reflective grating and echelon mirror. Experimental results show that the echelon mirror configuration achieves a 0.4% conversion efficiency and a 51.7 mW average THz power, exceeding the performance of the grating configuration, which reaches 0.26% and 41.8 mW, respectively. These results confirm that combining short pulses with the echelon mirror enhances both conversion efficiency and average THz power under high-power pumping, providing experimental guidance for high-power strong-field THz sources for material manipulation and biomedical imaging.

Keywords: echelon-based tilted-pulse-front pumping; grating-based tilted-pulse-front pumping; high-power laser; lithium niobate terahertz source

1. Introduction

Terahertz (THz) radiation, with its unique spectral characteristics, has significant potential for applications in materials science[1,2], biomedicine[3–7] and ultrafast spectroscopy[8–10]. In particular, strong-field THz sources can induce nonlinear responses in materials[11–13] and enable advanced research such as THz-driven electron acceleration[14–16] and higher-harmonic generation[17,18]. Using large-scale Ti:sapphire laser systems, researchers have achieved millijoule-level strong-field THz radiation[19–21], providing a powerful tool for extreme THz manipulation of matter. However, these systems operate at low repetition rates (typically $\leq$1 kHz) and require large, complex setups. These limitations restrict their use in applications that require high repetition rate, high average power and high beam quality, such as angle-resolved photoemission spectroscopy (ARPES), scanning near-field optical microscopy (SNOM) and high-resolution THz imaging[22–26]. The primary challenge in this field is developing THz sources capable of delivering high repetition rate, high average power and field strength above 100 kV/cm, while maintaining high efficiency, stability and beam quality.

Tilted-pulse-front pumping (TPFP) in lithium niobate (LN) crystals has become a leading approach for generating high-intensity, high-power THz radiation. TPFP improves optical rectification efficiency by realizing phase matching between the pump pulse and the THz wave. Two main approaches are commonly used: diffraction-based manipulation with gratings[27,28] and reflection-based manipulation with echelon mirrors[29,30]. The grating-based method provides high diffraction efficiency but introduces angular dispersion, leading to temporal stretching of the pump pulse. In contrast, the echelon mirror-based approach

Correspondence to: X. Wu, Hangzhou International Innovation Institute, Beihang University, Hangzhou 311115, China. Email: xiaojunwu@buaa.edu.cn

†These authors contributed equally to this work.

© The Author(s), 2026. Published by Cambridge University Press in association with Chinese Laser Press. This is an Open Access article, distributed under the terms of the Creative Commons Attribution licence (https://creativecommons.org/licenses/by/4.0), which permits unrestricted re-use, distribution and reproduction, provided the original article is properly cited.

Downloaded from https://www.cambridge.org/core. 18 Nov 2026 at 07:41:54, subject to the Cambridge Core terms of use.

avoids angular dispersion but generally yields a lower conversion efficiency, as reported in previous studies. Thus, selecting the optimal TPFP scheme to maximize conversion efficiency and average power under specific pump laser parameters remains a key scientific challenge.

In recent years, the development of high-average-power ytterbium-doped lasers has provided an ideal pump source for high-repetition-rate, high-power THz generation[31–33]. Meanwhile, THz sources based on ytterbium-doped lasers have achieved remarkable progress in average power[34–38]. However, commercial ytterbium lasers generally have long pulse durations (>500 fs) and limited single-pulse energy, limiting further improvement of peak power density and nonlinear conversion efficiency. These factors directly constrain the achievable peak power density and nonlinear conversion efficiency. Previous studies have shown that under long-pulse, low-energy pumping conditions, grating-based schemes exhibit higher efficiency than echelon mirror configurations. However, recent studies have achieved a record room-temperature conversion efficiency of 1.3% using an echelon mirror scheme with approximately 280 fs pump pulses and approximately 400 μJ single-pulse energy[39]. Combined with previous long-pulse duration work, this result indicates that high conversion efficiency in TPFP systems can be obtained at limited single-pulse energy by optimizing the pump pulse duration and the phase-matching condition. However, at higher single-pulse energies, the efficiency, spot size and thermal management must be optimized simultaneously. This study focuses on the high-energy regime and aims to explore how to improve efficiency by shortening the pulse duration at millijoule-level pump energies, while systematically evaluating the performance of the grating and echelon mirror schemes under this condition.

To address these challenges, a high-power ytterbium-doped femtosecond laser operating at 1035 nm (2 mJ pulse energy, 226 fs pulse duration, 10 kHz repetition rate) was used. Two TPFP schemes – a reflective grating and a reflective echelon mirror – were experimentally compared for THz generation in LN at room temperature. Experimental results indicate that reducing the pump pulse duration effectively enhances the conversion efficiency. Compared with previous studies reporting lower efficiency for the echelon mirror scheme, this work achieved a significant enhancement in conversion efficiency, reaching 0.4% for the echelon mirror and 0.26% for the grating scheme by shortening the pulse duration to 226 fs. The results demonstrate this effect in the high-energy regime. At mJ-level pump energies, reducing the pulse duration from more than 500 fs to approximately 226 fs increases peak power density and significantly enhances the conversion efficiency of both the echelon mirror and grating TPFP schemes. Although the extremely high conversion efficiency achieved under low-energy pumping cannot be maintained at higher pump energies, the echelon mirror configuration delivers better overall performance, reaching 0.4% conversion efficiency and 51.7 mW average power, both of which are higher than the grating scheme under identical conditions. This result confirms that, under high single-pulse energy conditions, short-pulse pumping and the echelon mirror scheme provide an effective approach for achieving high efficiency and high-average-power output. This work systematically characterizes the performance limits of the two TPFP schemes in this important parameter range and provides clear experimental guidance for the design of high-power THz sources.

2. Working principle

The experiment employed an industrial-grade ytterbium-doped solid-state laser (Y-Laser, HELIOS-20W-HE) operating at a center wavelength of 1035 nm with a spectral bandwidth of approximately 10 nm. The pulse duration was tunable from 226 fs to 10 ps. During the experiment, the laser system operated at a repetition rate of 10 kHz, delivering single-pulse energies of more than 2 mJ and an average output power of more than 20 W. A continuously adjustable attenuation module, composed of a half-wave plate and a polarizer, was installed in the optical path to control the energy incident on the THz generation module. The laser produced horizontally polarized radiation and exhibited near-diffraction-limited beam quality with $M^2 \approx 1.1 \times 1.1$. The beam diameter was approximately 5.3 mm ($1/e^2$), as shown in Figure 1(b), and the power stability was better than 0.12% root mean square (RMS) over 24 hours of continuous operation.

Figure 1(a) shows a schematic of the experimental setup. The laser output was split by a polarization isolation system into two beams according to the desired energy ratio. About 90% was used for THz generation, and 10% was sent to an optical parametric amplifier (Y-Laser, AURORA-H-HP) as the probe seed. The amplifier outputs a signal radiation tunable from 650 to 900 nm, as shown in Figure 1(d). The 850 nm signal served as the probe beam. After compression by a fused silica prism pair, the pulse duration was reduced to 43 fs, improving the sensitivity of THz field detection, as shown in Figure 1(c).

For the grating-based scheme, the pump beam first passed through a 1.5× Galilean expander composed of a concave lens (f = –50 mm) and a convex lens (f = 75 mm) to reduce the optical intensity on subsequent components. The expanded beam was then directed onto a reflective grating (1200 grooves/mm) to generate a tilted-pulse-front via diffraction. The –1st-order diffracted beam was subsequently directed into a 4-f imaging system consisting of 250 and 100 mm achromatic lenses, which imaged the tilted-pulse-front onto the LN crystal surface. In addition, for the echelon mirror

Downloaded from https://www.cambridge.org/core. 18 Nov 2026 at 07:41:54, subject to the Cambridge Core terms of use.

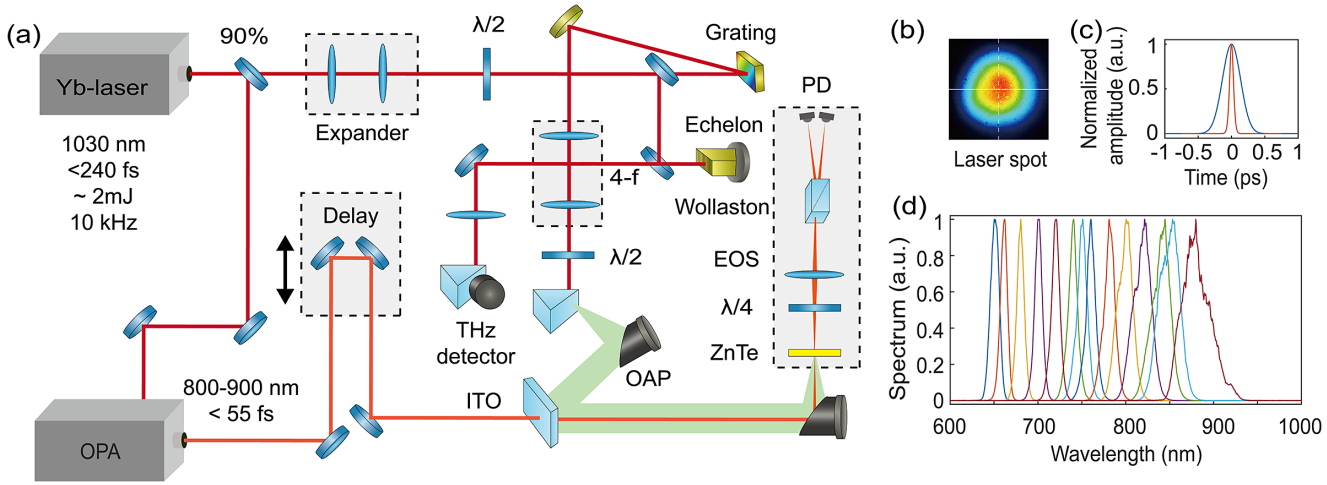


Figure 1. Experimental optical path diagram and laser parameters. (a) Optical path diagrams for the grating-based and the echelon mirror-based tilted-pulse-front pumping. (b) Laser spot output by the 20 W laser (~5.3 mm ($1/e^2$)). (c) Pump pulse duration (blue line) and signal light pulse duration (red line). (d) Signal optical spectrum.

scheme, the pump beam was first expanded using either the 1.5× Galilean expander described above or an alternative 2.5× expander composed of –50 and 125 mm lenses. The expanded beam was then directed perpendicularly onto a reflective echelon mirror consisting of 75 uniform steps (187 μm width, 85 μm height, ~90% reflectivity at 1035 nm) using a flip mirror. The reflected beam, carrying a discretely tilted pulse front defined by the step geometry, was focused by a 100 mm achromatic lens after 550 mm of free-space propagation, with the LN crystal positioned approximately 121 mm behind the lens.

The THz generation medium was a 5% MgO-doped LN crystal, fabricated into an isosceles prism with 63° edge angle, 20 mm waist length and 30 mm height, optimized for TPFP operation. The incident surface was coated with an antireflection layer optimized for 1035 nm to minimize pump reflection losses. The crystal was mounted on a three-dimensional precision stage to ensure precise pump alignment. The generated THz radiation is emitted from the output facet of the LN crystal. Different collection optics are employed to accommodate the distinct divergence characteristics of the two schemes. The focal spot sizes and peak electric fields reported for the two configurations are not directly comparable in a strict one-to-one sense, as different collection optics were adopted to optimally match the individual divergence behavior of each scheme. The relatively low divergence of the grating-based scheme permits the use of a 4-inch focal length off-axis parabola (OAP) for collimation and a 2-inch OAP for focusing. In contrast, the higher divergence of the echelon-based scheme requires a 2-inch collection OAP and a 4-inch focusing OAP to maximize the THz collection efficiency. These optical configurations were selected to independently optimize the performance of each scheme, and the reported focal spot sizes and peak fields represent the actual performance achieved under each optimized system configuration.

The THz output was characterized in terms of energy, time-domain waveform and beam profile. The THz energy was measured using a custom-designed high-sensitivity pyroelectric detector (Gentec-EO, SDX-1152-MT) placed directly behind the crystal output facet. To ensure accurate comparison between configurations, a calibrated filter array was placed before the detector to control attenuation. For the grating-based scheme, a 1 mm high-resistivity silicon wafer and a 20 μm black polyimide film were used, providing a total attenuation of approximately 70%. For the echelon mirror-based scheme, a 1-mm high-resistivity silicon wafer, a 1 mm black high-density polyethylene (HDPE) film and a 1 mm alumina ceramic film were used, providing a total attenuation of approximately 49%. All reported THz power and energy values were corrected according to these attenuation coefficients.

The time-domain waveform was measured by electro-optic sampling using a balanced detection configuration to enhance the dynamic range. The collimated THz beam was reflected by indium tin oxide (ITO) glass and subsequently focused onto a 500-μm-thick, <110>-cut ZnTe crystal with a second off-axis parabolic mirror. The 43-fs 850-nm probe beam from the optical parametric amplifier passed through the ITO glass and temporally overlapped with the THz pulses inside the ZnTe crystal after an electric delay stage, enabling electro-optic THz field detection. To modulate THz signals and improve the signal-to-noise ratio, a 1 kHz optical chopper was placed in the pump beam path for modulation, and the signal was demodulated using a lock-in amplifier (Zurich Instruments, MFLI). The spatial profile of the THz beam was measured with a THz camera (Ophir: PY-III-HR-C-A-PRO) positioned at the focal plane of the second

Downloaded from https://www.cambridge.org/core. 18 Nov 2026 at 07:41:54, subject to the Cambridge Core terms of use.

off-axis parabolic mirror. All experiments were performed in a temperature-controlled environment at 22°C and a relative humidity of 54%.

3. Results and analysis

To evaluate the performance of short-pulse-pumped TPFP, a reflective grating-based system was constructed and optimized. A reflective grating with a groove density of 1200 grooves/mm was used to generate the tilted pulse front, and the geometric parameters of the grating were designed such that the diffraction angle differs from the incident angle by 10°. According to the grating equation $d[\sin(i)+\sin(\theta)]=m\lambda$, when the pump beam is incident at 33.6°, the −1st-order diffracted beam emerges at 43.6°, with a measured diffraction efficiency of 97%. The angular dispersion introduced by the grating spatially separates the spectral components of the pump beam, thereby generating a continuous linearly tilted pulse front. The initial tilted-pulse-front angle γ'' is determined by the angular dispersion relation $\tan(\gamma'')=-k\frac{\mathrm{d}\theta}{\mathrm{d}k}$, where $\frac{\mathrm{d}\theta}{\mathrm{d}k}$ is the angular dispersion rate of the grating, which is associated with the grating equation.

Subsequently, this tilted pulse front is guided into a 4-f imaging system, where the initial tilt angle is transformed by the beam reduction ratio M of the 4-f imaging system, following the relation $\tan(\gamma')=M\tan(\gamma'')$, where γ' is the tilt angle outside the crystal after imaging. When the pump beam is normally incident on the LN crystal, due to the crystal refractive index $n\approx 2.2$, the tilted pulse front refracts at the crystal interface, and the effective tilt angle γ inside the crystal satisfies $\tan(\gamma)=\frac{\tan(\gamma')}{n}$. To achieve phase matching for THz generation, the tilt angle γ inside the crystal must satisfy $V_{\mathrm{THz}}=V_{\mathrm{g}}\cos(\gamma)$, where V_{THz} is the THz phase velocity and V_{g} is the pump group velocity. Substituting the refractive index and dispersion characteristics of LN, the γ value satisfying phase matching is calculated to be approximately 63°. The base angle of the LN crystal is designed to be consistent with this tilt angle; thus, under the phase-matching condition, the pump tilted pulse front is designed to be parallel to the THz exit surface of the LN crystal, and the generated THz radiation propagates perpendicular to the pump pulse front, ultimately emitting perpendicular to the crystal exit surface.

Based on the above phase-matching mechanism, the beam reduction ratio M satisfying the optimal matching condition can be derived, with its expression given by $\tan(\gamma)=\frac{mM\lambda}{nd\cos(\theta)}$. Substituting our experimental parameters ($\lambda=1035$ nm, $n\approx 2.2$, $d=1/1200$ mm, $\theta=43.6°$) yields a scaling ratio $M\approx 2.5$ for the 4-f system. The experimental configuration agrees well with theoretical calculations, ensuring effective phase matching. Meanwhile, the 4-f system compensates for the angular dispersion introduced by the grating, suppressing spatiotemporal broadening of the pump pulse and preserving its high-peak-power density.

The THz output energy of the grating scheme was characterized as a function of pump energy, with the laser operating at a 10 kHz repetition rate and a pulse duration of 226 fs, as shown in Figure 2(b). The THz pulse energy increased almost linearly from 0.19 to 4.18 μJ as the pump energy increased from 0.16 to 1.6 mJ. The maximum optical-to-THz conversion efficiency of 0.26% was achieved at 1.44 mJ pump energy, corresponding to a THz pulse energy of 3.79 μJ. This efficiency is significantly higher than that obtained under long-pulse (>500 fs) pumping, confirming that short pulses enhance conversion efficiency by increasing the peak power density. The inset of Figure 2(b) shows the THz focal spot, with full widths at half maximum (FWHMs) of 0.68 and 0.60 mm along the two axes. From the measured spot size and energy, the peak electric field at the focus was estimated to be approximately 680 kV/cm.

Figure 2(c) shows the THz temporal waveform measured at a 10-kHz repetition rate, exhibiting a typical single-cycle pulse. The corresponding spectrum, obtained by Fourier transform, is presented in Figure 2(d). The spectrum spans from 0.1 to 3 THz with a center frequency of 0.54 THz. A distinct dip at 0.55 THz originates from water vapor absorption in the ambient environment. The measurement system exhibits a dynamic range of 58 dB, demonstrating high detection sensitivity.

4. Tilted-pulse-front pumping terahertz generation based on a reflective echelon mirror

For comparison, a reflective echelon-based TPFP configuration was developed and optimized. The corresponding operating principle is illustrated in Figure 3(a). As mentioned above, the echelon mirror used in this study consists of uniform steps with a width of 187 μm and a height of 85 μm. The pump beam, incident perpendicularly on the echelon mirror, is reflected and divided into a sequence of time-delayed sub-pulses, forming a discrete tilted pulse front. The initial tilt angle is determined by the step geometry and can be calculated as $\theta=\arctan\left(\frac{2H}{W}\right)=42.3°$. This discrete tilted pulse front is imaged onto an LN crystal through an achromatic imaging lens with a focal length of 100 mm.

For the echelon-based TPFP configuration, the effective tilt angle γ inside the crystal is related to the beam reduction ratio M by the relation $\gamma=\arctan\left(\frac{2HM}{Wn}\right)$. This formula incorporates the refraction effect at the crystal interface, where n is the refractive index of LN, ensuring that the calculation results meet the phase-matching requirements. By setting $\gamma=63°$ and substituting $H=85$ μm, $W=187$ μm and $n\approx 2.2$, the theoretically required beam-shortening ratio is calculated to be $M=4.85$. Thus, the LN crystal was positioned 121 mm behind the imaging lens, ensuring that the effective tilt angle of the pump pulse front inside the

Downloaded from https://www.cambridge.org/core. 18 Nov 2026 at 07:41:54, subject to the Cambridge Core terms of use.

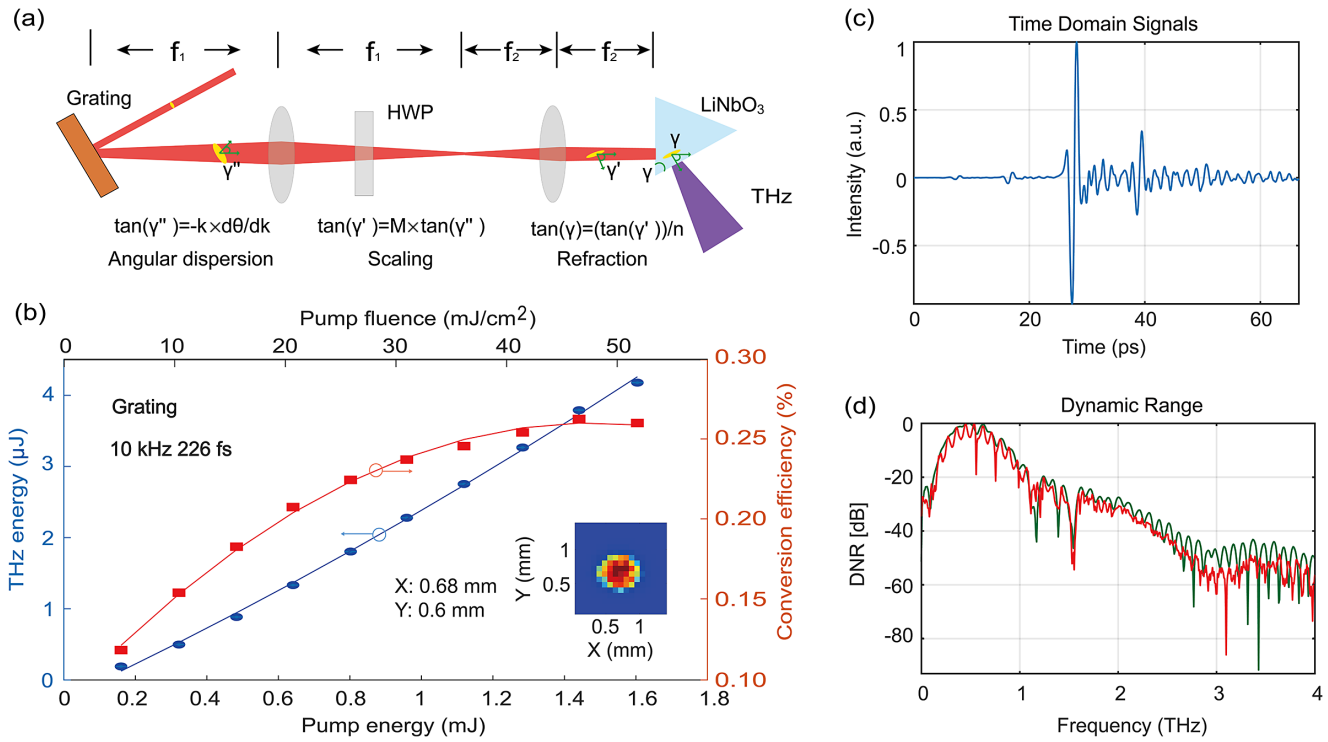


Figure 2. Grating scheme. (a) Schematic diagram of the TPFP principle using the grating scheme. (b) THz energy and conversion efficiency as a function of pump energy measured using the grating scheme. (c) Time-domain waveform of THz radiation generated by the grating scheme. (d) Spectrum of THz radiation generated by the grating scheme (red), where the green line represents the spectrum after removing echoes.

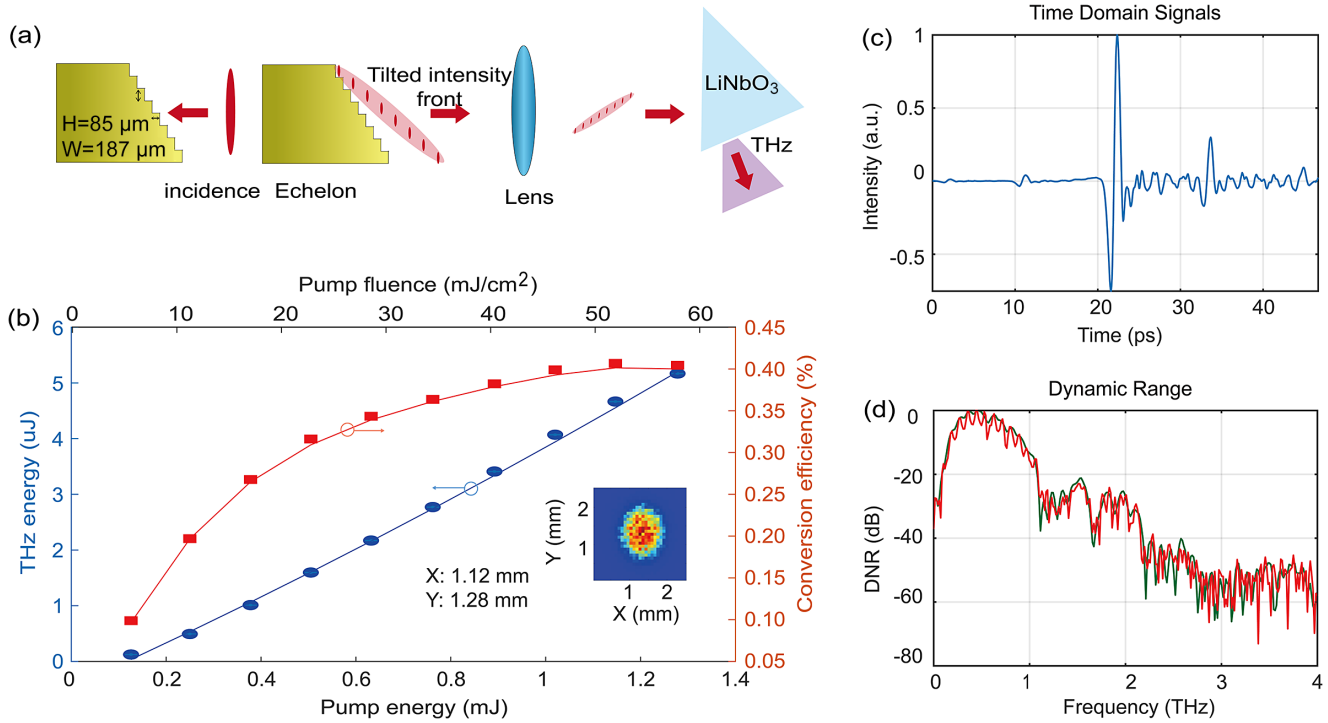


Figure 3. Echelon mirror scheme. (a) Schematic diagram of the TPFP principle using the echelon mirror. (b) THz energy conversion efficiency as a function of pump energy measured using the echelon mirror scheme. (c) Time-domain waveform of the THz energy generated by the echelon mirror scheme. (d) Spectrum of the THz energy generated by the echelon mirror scheme, where the green line represents the spectrum after reflection signal removal.

crystal matched the 63° base angle. This configuration satisfied the phase-matching condition required for efficient THz generation via optical rectification. Furthermore, since the step width (187 μm) is much larger than the pump wavelength (1.03 μm), the diffraction effect is negligible. As a result, each sub-pulse preserves the temporal profile of

Downloaded from https://www.cambridge.org/core. 18 Nov 2026 at 07:41:54, subject to the Cambridge Core terms of use.

the original pump pulse, ensuring high-peak-power density during propagation. Simultaneously, the step height introduces a delay of $\Delta t = \frac{2H}{c} = 567$ fs between adjacent pulses. The time delay is considerably smaller than the oscillation period of a THz wave, enabling coherent superposition of the radiation from all sub-pulses and thereby improving conversion efficiency.

The results for the echelon mirror scheme are shown in Figure 3(b). With a pulse duration of 250 fs and a repetition rate of 10 kHz, the THz energy increased with pump energy, reaching 4.66 μJ at 1.15 mJ, corresponding to a maximum conversion efficiency of 0.4%, which exceeds that of the grating scheme. These results further verify the effectiveness of short-pulse pumping. Nevertheless, the maximum pump energy attainable in the echelon mirror configuration (1.28 mJ) was lower than that of the grating-based system. This can be attributed to two primary factors; the echelon mirror exhibits lower reflectivity (~90%) than the grating's diffraction efficiency (>97%), and partial beam energy is lost due to beam clipping along the optical path. The inset of Figure 3(b) shows a larger focal spot (1.12 mm × 1.28 mm) compared with the grating scheme. This is primarily attributed to differences in the THz collection optics between the two schemes.

Figures 3(c) and 3(d) show the THz time-domain waveform and corresponding spectrum of the echelon mirror scheme, respectively. The waveform exhibits a single-cycle pulse. The spectrum extends from 0.1 to 2.3 THz, centered around 0.44 THz, with a distinct absorption feature at 0.55 THz attributed to water vapor. The measurement system provides a dynamic range of 50 dB.

For these two different TPFP schemes, the functional relationship between conversion efficiency and pump fluence was analyzed to ensure that the comparison between them is not affected by differences in pump intensity. For the grating scheme, the maximum efficiency of 0.26% was achieved at a pump fluence of approximately 46 mJ/cm^2. For the echelon mirror scheme under the 1.5× beam expansion configuration, the beam diameter at the crystal was too small, resulting in a pump fluence of 167 mJ/cm^2 at the maximum efficiency point, and the pump fluence is close to the crystal damage threshold, where an excessively high fluence causes crystal damage and pronounced nonlinear absorption. For the 2.5× beam expansion configuration, a conversion efficiency of 0.4% was achieved for the echelon mirror scheme, with a pump energy of 1.15 mJ and a pump fluence of approximately 52 mJ/cm^2. The higher fluence in the echelon scheme is a direct consequence of its larger beam compression ratio ($M = 4.85$ versus $M = 2.5$ for the grating), which was necessary to achieve the required phase-matching condition. Importantly, at a comparable fluence level of approximately 46 mJ/cm^2, the echelon-based scheme still outperforms the grating-based scheme, achieving a conversion efficiency of 0.39%, compared with 0.26% for the grating-based scheme. This confirms that the superior performance of the echelon mirror scheme originates from its intrinsic advantages, including the absence of angular dispersion and the preservation of short pulse durations, rather than simply operating at a higher pump fluence.

5. Impact of pump parameters on terahertz generation

To further investigate the influence of pump parameters on THz conversion efficiency, the distinct effects of pump pulse duration and incident pump power on the THz generation performance were systematically examined for both grating and echelon mirror TPFP configurations. Figure 4(a) presents the measured dependence of single-pulse THz energy on pump pulse duration under the fixed high-power pumping condition of millijoule-level single-pulse energy, which directly reflects the correlation between pulse temporal characteristics and optical rectification efficiency. For the grating-based TPFP scheme, the single-pulse THz energy decreases sharply with the increase of pump pulse duration, a trend that clearly indicates that longer pump pulses lead to a significant reduction in the peak power density of the pump beam, which in turn is the key factor limiting the nonlinear optical rectification efficiency and thus the THz energy output.

For the echelon mirror scheme, under the larger spot size condition with 2.5× beam expansion, the corresponding pump fluence on the LN crystal is relatively low. As the pump pulse duration is extended from 226 to 250 fs, the single-pulse THz energy exhibits a slight but measurable increase, followed by a continuous and gradual decline with further lengthening of the pulse duration. This distinctive initial rising trend deviates from the conventional expectation that longer pulses reduce conversion efficiency, and can be attributed to strong nonlinear multiphoton absorption induced by the elevated pump power density at excessively short pulse durations. In contrast, a moderate extension of the pulse duration to 250 fs reasonably reduces the pump power density and suppresses multiphoton absorption as well as pump energy loss, leading to a slight increase in THz energy. Beyond this point, the dominant effect of reduced peak power density governs the conversion efficiency for longer pulses. However, under the condition of a small focal spot size with 1.5× beam expansion, the corresponding pump fluence is comparatively high. The single-pulse THz energy drops rapidly as the pump pulse duration increases from 226 to 700 fs, and then stabilizes at a relatively constant value between 700 and 1100 fs. The observed plateau in the THz energy curve indicates that the prolonged pump pulse duration effectively increases the effective spatiotemporal interaction length between the pump beam and the LN crystal for optical rectification, which partially compensates for the efficiency loss caused by the reduced peak power

Downloaded from https://www.cambridge.org/core. 18 Nov 2026 at 07:41:54, subject to the Cambridge Core terms of use.

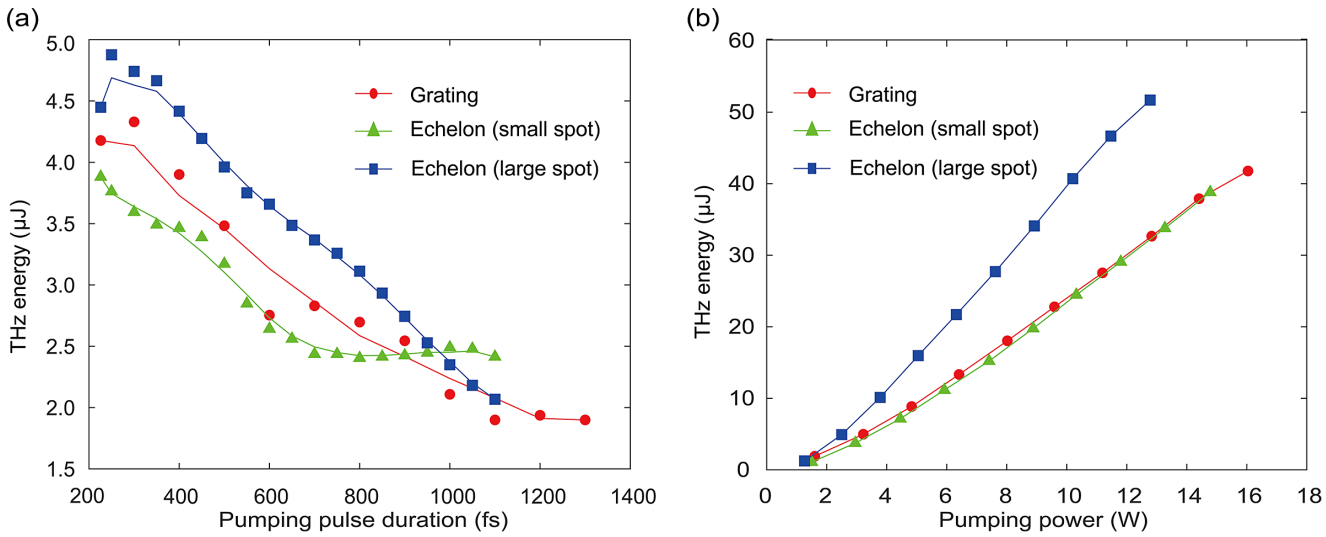


Figure 4. Effect of pump pulse duration and power on conversion efficiency. (a) Impact of pulse duration variation on single-pulse THz energy. (b) Influence of pump power and spot size on single-pulse THz energy.

Table 1. Comparison of high-power lithium niobate terahertz sources at room temperature[34,37,39,40].

Reference	Pump pulse duration	Max. pump energy	Rep. rate	Pump power	Avg THz power	Efficiency
Meyer *et al.* 2020[34]	<100 fs	9.2 μJ	13.3 MHz	110 W	66 mW	~0.1%
Guiramand *et al.* 2022[39]	280 fs	400 μJ	25 kHz	10 W	74 mW	1.3%
Kong *et al.* 2025[37]	570 fs	1 mJ	50 kHz	50 W	66.7 mW	0.2%
Xu *et al.* 2025[40]	1 ps	2 mJ	100 kHz	200 W	104 mW	0.1%
This work (grating)	**226 fs**	**2 mJ**	**10 kHz**	**20 W**	**41.8 mW**	**0.26%**
This work (echelon)	**250 fs**	**2 mJ**	**10 kHz**	**20 W**	**51.7 mW**	**0.4%**

density. Notably, under this small-spot condition, the pump fluence on the LN crystal surface at the shortest pulse duration of 226 fs approaches the material damage threshold, which inherently limits the maximum achievable THz energy output under this optimal short-pulse parameter set.

Figure 4(b) compares the variation of THz average power with pump power for the three configurations. In all cases, the THz power increases approximately linearly with pump power. Among the three schemes, the larger spot size echelon mirror configuration achieved the highest THz average power of 51.7 mW, while the grating scheme reached 41.8 mW. These results demonstrate that, under the short-pulse, high-energy pump conditions investigated in this work, the echelon mirror-based TPFP scheme is more effective in generating higher average power output.

In order to further evaluate the performance of the present work, Table 1 systematically summarizes the key characteristics of state-of-the-art high-power LN THz sources operating at room temperature in recent works, including pumping parameters (pulse duration, pulse energy, repetition rate), achieved conversion efficiency and average THz power. Several conclusions can be drawn from this comparison.

Several observations can be drawn from this comparison. Firstly, at lower pump energies (<500 μJ), extremely high conversion efficiencies (>1%) can be achieved, representing the limit of efficiency optimization in the low-energy regime. Secondly, at higher pump energies (mJ level), the trade-off between conversion efficiency and output power becomes evident. For systems aiming to achieve high average power, cooling or operating at a lower efficiency is often necessary. Thirdly, our work demonstrates that shortening the pump pulse duration to approximately 250 fs at mJ-level single-pulse energy significantly enhances the optical rectification efficiency in LN. Compared with long-pulse pumping (>500 fs), the conversion efficiency is nearly doubled under otherwise comparable conditions. Fourthly, under room-temperature, mJ-level pumping with short pulses (~250 fs), the echelon mirror scheme achieves a favorable balance between conversion efficiency (0.4%) and average power (51.7 mW), outperforming the grating scheme under identical conditions. This positions our approach as a valuable reference for applications requiring both high pulse energy and high average power without cryogenic cooling.

6. Conclusion

In this work, we systematically compare THz generation via TPFP with reflective gratings and echelon mirrors under short-pulse (~226 fs) and high-energy (mJ-level)

Downloaded from https://www.cambridge.org/core. 18 Nov 2026 at 07:41:54, subject to the Cambridge Core terms of use.

pumping from a high-average-power ytterbium-doped laser. Experimental results show that under high-energy, short-pulse conditions, the echelon mirror scheme achieves a conversion efficiency of 0.4% and an average THz power of 51.7 mW, outperforming the grating scheme (0.26%, 41.8 mW). This advantage arises from the echelon mirror's ability to suppress angular dispersion while preserving the high peak power of short pulses. Relative to previous long-pulse (>500 fs) studies, our schemes demonstrate improved efficiency, indicating that shortening the pulse duration to raise peak power density is an effective strategy for overcoming the nonlinear conversion bottleneck at high pump energies. Although the grating scheme offers slightly better beam focusing, the results indicate that for high-energy THz generation, short-pulse pumping combined with the echelon mirror scheme yields higher conversion efficiency and average power, making this combination the preferred approach. This work provides reliable experimental data for THz generation under high-power, short-pulse and millijoule-level single-pulse pumping conditions. It systematically reveals the performance differences and applicability of the grating and echelon mirror schemes, clarifying the factors that limit THz generation efficiency. These results offer key guidance for designing high-power intense THz sources with high-average-power output.

Acknowledgements

This work was supported by the Scientific Research Innovation Capability Support Project for Young Faculty (Grant No. ZYGXQNJSKYCXNLZCXM-I3), the National Key Research and Development Program of China (Grant No. 2022YFA1604402), the National Natural Science Foundation of China (Grant Nos. U23A6002 and 92250307) and the Beijing Municipal Science & Technology Commission, Administrative Commission of Zhongguancun Science Park (Grant No. Z251100006925005).

References

1. R. Salikhov, I. Ilyakov, L. Körber, A. Kákay, R. Gallardo, A. Ponomaryov, J. Deinert, T. de Oliveira, K. Lenz, J. Fassbender, S. Bonetti, O. Hellwig, J. Lindner, and S. Kovalev, Nat. Phys. **19**, 529 (2023).
2. T. Kampfrath, K. Tanaka, and K. Nelson, Nat. Photonics **7**, 680 (2013).
3. K. Ajito and Y. Ueno, IEEE Trans. Terahertz Sci. Technol. **1**, 293 (2011).
4. X. Chen, H. Lindley-Hatcher, R. Stantchev, J. Wang, K. Li, A. Serrano, Z. Taylor, E. Castro-Camus, and E. Pickwell-MacPherson, Chem. Phys. Rev. **3**, 011311 (2022).
5. K. Okada, K. Serita, Q. Cassar, H. Murakami, G. MacGrogan, J. Guillet, P. Mounaix, and M. Tonouchi, J. Phys. Photonics **2**, 044008 (2020).
6. A. Markelz and D. Mittleman, ACS Photonics **9**, 1117 (2022).
7. K. Zaytsev, I. Dolganova, N. Chernomyrdin, G. Katyba, A. Gavdush, O. Cherkasova, G. Komandin, M. Shchedrina, A. Khodan, D. Ponomarev, I. Reshetov, V. Karasik, M. Skorobogatiy, V. Kurlov, and V. Tuchin, J. Opt. **22**, 013001 (2020).
8. H. Hwang, S. Fleischer, N. Brandt, B. Perkins, M. Liu, K. Fan, A. Sternbach, X. Zhang, R. Averitt, and K. Nelson, J. Mod. Opt. **62**, 1447 (2015).
9. K. Tanaka, H. Hirori, and M. Nagai, IEEE Trans. Terahertz Sci. Technol **1**, 301 (2011).
10. P. Jepsen, D. Cooke, and M. Koch, Laser Photonics Rev. **5**, 124 (2011).
11. Y. Lu, Y. Huang, J. Cheng, R. Ma, X. Xu, Y. Zang, Q. Wu, and J. Xu, Nano **13**, 3279 (2024).
12. M. Liu, H. Hwang, H. Tao, A. Strikwerda, K. Fan, G. Keiser, A. Sternbach, K. West, S. Kittiwatanakul, J. Lu, S. Wolf, F. Omenetto, X. Zhang, K. Nelson, and R. Averitt, Nature **487**, 345 (2012).
13. X. Li, T. Qiu, J. Zhang, E. Baldini, J. Lu, A. Rappe, and K. Nelson, Science **364**, 1079 (2019).
14. D. Zhang, A. Fallahi, M. Hemmer, X. Wu, M. Fakhari, Y. Hua, H. Cankaya, A. Calendron, L. Zapata, N. Matlis, and F. Kärtner, Nat. Photonics **12**, 336 (2018).
15. X. Yu, Y. Zeng, L. Song, D. Kong, S. Hao, J. Gui, X. Yang, Y. Xu, X. Wu, Y. Leng, Y. Tian, and R. Li, Nat. Photonics **17**, 957 (2023).
16. W. Huang, A. Fallahi, X. Wu, H. Cankaya, A. Calendron, K. Ravi, D. Zhang, E. Nanni, K. Hong, and F. Kärtner, Optica **3**, 1209 (2016).
17. M. Hohenleutner, F. Langer, O. Schubert, M. Knorr, U. Huttner, S. Koch, M. Kira, and R. Huber, Nature **523**, 572 (2015).
18. K. Kovács, E. Balogh, J. Hebling, V. Tosa, and K. Varjú, Phys. Rev. Lett. **108**, 193903 (2012).
19. X. Wu, D. Kong, S. Hao, Y. Zeng, X. Yu, B. Zhang, M. Dai, S. Liu, J. Wang, Z. Ren, S. Chen, J. Sang, K. Wang, D. Zhang, Z. Liu, J. Gui, X. Yang, Y. Xu, Y. Leng, Y. Li, L. Song, Y. Tian, and R. Li, Adv. Mater. **35**, 2208947 (2023).
20. J. Fülöp, Z. Ollmann, C. Lombosi, C. Skrobol, S. Klingebiel, L. Pálfalvi, F. Krausz, S. Karsch, and J. Hebling, Opt. Express **22**, 20155 (2014).
21. B. Zhang, Z. Ma, J. Ma, X. Wu, C. Ouyang, D. Kong, T. Hong, X. Wang, P. Yang, L. Chen, Y. Li, and J. Zhang, Laser Photonics Rev. **15**, 2000295 (2021).
22. J. Reimann, S. Schlauderer, C. Schmid, F. Langer, S. Baierl, K. Kokh, O. Tereshchenko, A. Kimura, C. Lange, J. Güdde, U. Höfer, and R. Huber, Nature **562**, 396 (2018).
23. T. Cocker, V. Jelic, R. Hillenbrand, and F. Hegmann, Nat. Photonics **15**, 558 (2021).
24. T. Cocker, V. Jelic, M. Gupta, S. Molesky, J. Burgess, G. De Los Reyes, L. Titova, Y. Tsui, M. Freeman, and F. Hegmann, Nat. Photonics **7**, 620 (2013).
25. X. Li, J. Li, Y. Li, A. Ozcan, and M. Jarrahi, Light Sci. Appl. **12**, 233 (2023).
26. P. Fosodeder, S. van Frank, and C. Rankl, Opt. Express **30**, 3684 (2022).
27. J. Hebling, G. Almási, I. Kozma, and J. Kuhl, Opt. Express **10**, 1161 (2002).
28. J. Hebling, K. Yeh, M. Hoffmann, B. Bartal, and K. Nelson, J. Opt. Soc. Am. B Opt. Phys. **25**, B6 (2008).
29. B. Ofori-Okai, P. Sivarajah, W. Huang, and K. Nelson, Opt. Express **24**, 5057 (2016).
30. Y. Minami, Y. Hayashi, J. Takeda, and I. Katayama, Appl. Phys. Lett. **103**, 051103 (2013).
31. U. Brauch, C. Röcker, T. Graf, and M. Ahmed, Appl. Phys. B Lasers Opt. **128**, 58 (2022).
32. T. Nubbemeyer, M. Kaumanns, M. Ueffing, M. Gorjan, A. Alismail, H. Fattahi, J. Brons, O. Pronin, H. Barros, Z. Major, T. Metzger, D. Sutter, and F. Krausz, Opt. Lett. **42**, 1381 (2017).

Downloaded from https://www.cambridge.org/core. 18 Nov 2026 at 07:41:54, subject to the Cambridge Core terms of use.

33. S. Esser, C. Röhrer, X. Xu, J. Wang, J. Zhang, T. Graf, and M. Ahmed, Opt. Lett. **46**, 6063 (2021).
34. F. Meyer, T. Vogel, S. Ahmed, and C. Saraceno, Opt. Lett. **45**, 2494 (2020).
35. P. Kramer, M. Windeler, K. Mecseki, E. Champenois, M. Hoffmann, and F. Tavella, Opt. Express **28**, 16951 (2020).
36. M. Abdo, S. Sheng, S. Rolf-Pissarczyk, L. Arnhold, J. Burgess, M. Isobe, L. Malavolti, and S. Loth, ACS Photonics **8**, 702 (2021).
37. D. Kong, Y. Su, C. Song, and X. Wu, Photonics Res. **13**, 2477 (2025).
38. T. Vogel, S. Mansourzadeh, and C. Saraceno, Opt. Lett. **49**, 4517 (2024).
39. L. Guiramand, J. Nkeck, X. Ropagnol, T. Ozaki, and F. Blanchard, Photonics Res. **10**, 340 (2022).
40. A. Xu, J. Li, D. Kong, J. Cai, T. Chen, D. Suthar, P. Cao, X. Yu, Y. Yang, M. Zhang, A. E. Moutaouakil, and X. Wu, Chin. Phys. Lett. **42**, 120406 (2025).

Downloaded from https://www.cambridge.org/core. 18 Nov 2026 at 07:41:54, subject to the Cambridge Core terms of use.